Isr. J. Earth Sci.; 49: 9–19

Experimental and theoretical investigations of electromagnetic radiation induced by rock fracture

Vladimir Frid,[a,b] Dov Bahat,[a,b] Julia Goldbaum,[a,c] and Avinoam Rabinovitch[a,c]
[a]The Deichmann Rock Mechanics Laboratory of the Negev, [b]Department of Geological and Environmental Sciences, and [c]Physics Department, Ben-Gurion University of the Negev, Be'er Sheva, Israel

(Received 6 December 1999; accepted 11 April 2000)

ABSTRACT

Frid, V., Bahat, D., Goldbaum, J., Rabinovitch, A. 2000. Experimental and theoretical investigations of electromagnetic radiation induced by rock fracture. Isr. J. Earth Sci. 49: 9–19.

There is a general agreement in the literature that the technique of measuring electromagnetic radiation (EMR) emitted from cracked rock is a good candidate for forecasting of earthquakes. Our immediate objective in pursuing this goal is to correlate EMR with crack dimensions in micro-scales (mm–cm), coupling it with the understanding of atomic-scale phenomena for coherently understanding the EMR process. We review some of the results obtained in this laboratory. They include the isolation, both experimentally and theoretically, of an individual EMR pulse. Individual EMR pulse parameters are correlated with crack dimensions: the time from pulse origin up to its maximum is proportional to the crack length, and the frequency of the EMR pulse relates to the crack width. Individual EMR pulses are classified both according to their length and according to their location on the stress–strain curve. We find that the key elastic parameter for EMR characterization during triaxial compression is the Poisson ratio: the lower the Poisson ratio, the higher the EMR activity. Amplitudes of EMR and their changes with loading are shown to be independent of crack mode (tensile vs. shear), they are only dependent on the entire crack area. In order to experimentally overcome load limitations we introduce a new sample shape, the truncated cone, that fails more readily than standard cylindrical samples.

INTRODUCTION

Electromagnetic radiation in fractured materials—experiments and theories

Emitted electromagnetic radiation (EMR) was first observed by Stepanov on fractured samples of sylvite (KCl) in 1933 (Urusovskaja, 1969). This study was followed by numerous others that investigated various aspects of EMR. The EMR phenomenon was measured for fracture in different materials, including metals and alloys (Misra, 1975; Jagasivamani and Iyer, 1988), single crystals (Gol'd et al., 1975; Khatiashvili, 1984), rocks (Nitsan, 1977; Warwick et al., 1982; Ogawa et al., 1985; O'Keefe and Thiel, 1995; Rabinovitch et al., 1995, 1996, 1998), and ice (Fifolt et al., 1993; Petrenko, 1993). In situ EMR is induced by mine rockbursts (Khatiashvili, 1984; Nesbitt, 1988;

E-mail: vfid@bgumail.bgu.ac.il

 0021-2164/00 $4.00

Frid 1997a,b). Thus, EMR is associated with fractures ranging over multiscale lengths and with various applications.

Several atomic-scale models have hitherto been suggested to explain the EMR phenomenon. All of these models were qualitative, and efforts to use EMR for quantitative fracture prediction were unsuccessful, due to the lack of a detailed quantitative understanding of the EMR phenomenon (King, 1983; Rabinovitch et al., 1998). Until now, the physical mechanism of EMR has been unknown. An essential requirement for this type of knowledge is a careful laboratory investigation of rock failure. Hence, the goal of our immediate investigation consisted of physically understanding the EMR process by carrying out an intensive experimental program.

EMR from rocks in connection with earthquake prognosis

During the 1970s and 1980s, interest in EMR increased in connection with the problem of earthquake (EQ) prognosis. As noted by Johnston (1991), several people observed a disruption of radio communications and an atmospheric luminescence before EQs. Sadovskii et al. (1979) observed an irregularity of EMR before some Carpathian EQs. Gokhberg et al. (1979) investigated EMR prior to an Iranian EQ. This study consisted of EMR registration at frequencies of 25, 385, and 1630 kHz, from a period of 55 min before the first EQ shock. EMR perturbations were observed to gradually increase up to the first shock moment. Following this shock, the levels at frequencies of 27 and 1630 kHz sharply decreased, but remained high at 385 kHz up to the last aftershock. These authors proposed that if the EMR sources were deposited in the earth's crust at the EQ epicenter, the original amplitude of the EMR signal would have to be of the order of hundreds of volts per meter. Similar investigations were also conducted in Japan (Gokhberg et al., 1982). EMR was registered at a distance of 250 km from the epicenter of an EQ of magnitude M = 7. Since an analysis of "industrial" noise showed its absence at a frequency of 81 kHz, that frequency was chosen for EMR studies. It was shown that 30 min before the EQ, the EMR amplitude rose by up to 15 dB and then sharply decreased at the EQ moment. EMR intensity (voltage) changes in a tunnel at a depth of about 60 m were also checked. Analysis of diurnal cycles of EMR intensity variations showed that they were significantly disturbed a few days before an EQ. Gokhberg et al. (1986) carried out measurements of EMR features prior to an EQ in Gasli, Uzbekistan. They found that 2 h 40 min before the EQ (M = 5), perturbations above the original noise level were increased by up to 6 dB. Yoshino and Tomizawa (1989) measured EMR (at a frequency of 82 kHz) before a volcanic eruption. The first EMR anomaly was registered two weeks before, and another powerful EMR emission (20 dB higher than the usual noise level) was observed one day prior to the eruption. Nikiforova and Yadakhin (1989) investigated EMR in the Issik-Kul, Kyrgyzstan seismic region at a frequency of 15 kHz. They obtained a significant increase of EMR intensity in the immediate zone of active geological faults, and claimed that the EMR sources were of ionosphere origin. On the other hand, Morgunov and Matveyev (1991) conducted an EMR investigation during the Spitak, Armenia EQ and claimed that EMR could not be explained as an ionosphere disturbance; its origin could only be ascribed to crust destruction. Gershen-zon et al. (1987, 1989) and Gokhberg et al. (1982, 1986) proposed that the anomalies of EMR prior to EQs were obtained by mechanical–electrical transformation. They noted that, before an EQ, a deformation of the earth's surface took place. Changes in the stress state of surfaces resulted in local destruction, in the formation of micro-fractures, and in friction of the nearby rock blocks. Each of these processes could lead to EMR generation. Bella et al. (1992), Morgunov (1985), Morgunov et al. (1988), and Morgunov and Matveyev (1990) also favored the idea that EMR was excited by surface deformation in the vast zone of the EQ vicinity. Gokhberg et al. (1985) noted the following principal features of EMR occurrences:

1. Abnormally high EMR levels occur hours, or even days, before an EQ.
2. The EQ itself takes place during a decrease of this EMR anomaly or immediately after it.
3. The EMR spectrum has a wide frequency range (from units Hz to hundreds kHz).

The third conclusion was also endorsed by Khatiashvili (1984) (who registered EMR in the range of 1–1000 kHz) and Bella et al. (1992) (who studied EMR in the range of 300 Hz–300 kHz). It is clear from the above papers that there is no uniquely accepted theory regarding the mechanism of EMR prior to an EQ. Parrot et al. (1993), after a detailed consideration of a large number of presently known EMR–EQ investigations, remarked that although the existence of EMR in relation to seismic and/or volcanic activities is clear, EMR selection out of a host of artificial signals

remains a significant problem. Nevertheless, investigations of EMR as a precursor to EQ are still in progress (Drakopoulos et al., 1993; Hayakawa et al., 1993, Yepez et al., 1995; Fujinawa and Takahashi, 1998), and presently there is agreement in the literature that EMR might be a prospective forecaster for EQs (King, 1983; Mogi, 1985; Yoshino et al., 1993). However, as we noted above, all efforts to use EMR for earthquake prediction met with very meager success, due to the lack of a detailed quantitative understanding of the EMR mechanism (King, 1983; Rabinovitch et al., 1996).

COMBINED EMR, ROCK MECHANICS, AND FRACTOGRAPHIC METHODS IN THE INVESTIGATION OF ROCK FRACTURE

Experimental equipment and method

The experimental setup is described in detail by Rabinovitch et al. (1998, 1999) and Frid et al. (1999). It consists of a "stiff" press, an antenna system, and the related electronics (Fig. 1). So far, we concentrated on uniaxial and triaxial compression tests on standard samples that were cut from blocks, with unified co-orientation, into standard cylinders of 100 mm in length and 53 mm in diameter. In addition, we introduced a new sample shape, the truncated cone, in our experiments (see below). Generally, the ends of the samples were scrupulously polished to get homogeneity of the stress field under compression. Each sample was tested by an axial strain rate of 1×10^{-5} s^{-1} and laterally by a different hydrostatic oil pressure.

Materials

This study focused on three distinct materials: chalk, granite, and glass-ceramic.

Chalk. Our samples were drilled from Middle Eocene layers along Wadi Naim in the Be'er Sheva syncline (Bahat, 1991). The density of all investigated samples was $2.16 \pm 0.01 \times 10^3$ kg/m^3. The strength of chalk under compression may vary considerably, from values of around 1 MPa when wet to some 50 MPa when extremely dry. Therefore, we applied a strict drying process to our samples, which involved a cycle of heating at 110 °C for 24 h, and then immediately removing to a desiccator, in order to avoid any water absorption by the samples. The axial loads varied from 30 MPa up to 60 MPa, and the confining pressure from 0 to 5 MPa.

Granite. For our investigation, we used a large Elat granite "block" from the Nahal Shelomo area of southern Israel, nearly 3 km from the city of Elat (Bogosh et

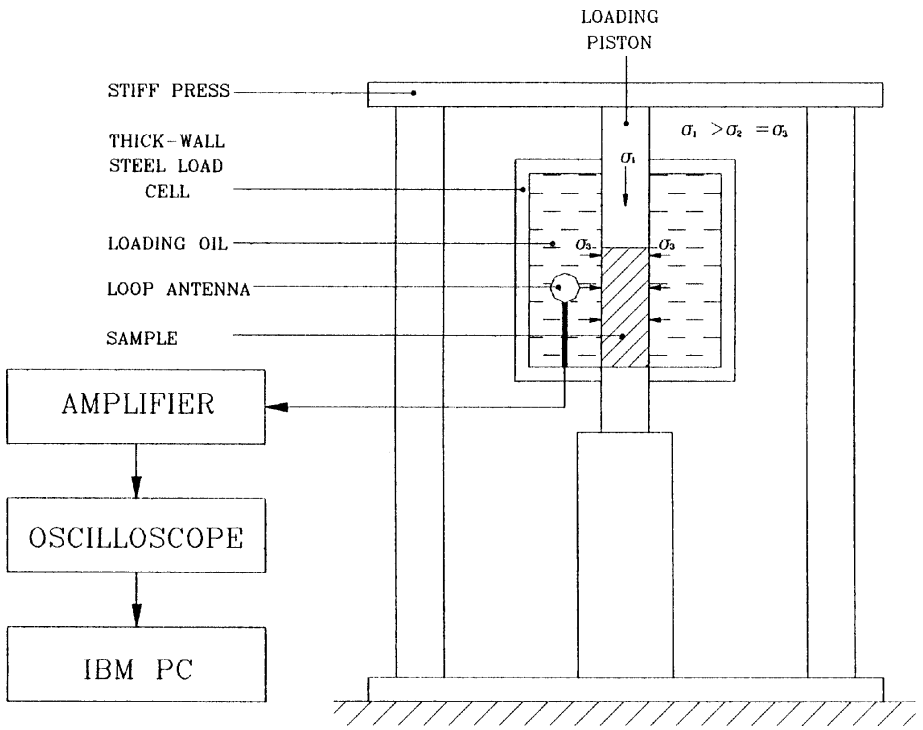

Fig. 1. Schematic diagram of experimental arrangement for measuring EMR of rock fracture.

al., 1997). The density of all investigated samples was $2.604 \pm 0.005 \times 10^3$ kg/m^3. The axial loads varied from 110 MPa up to 284 MPa, and the confining pressure from 0 to 14 MPa.

Glass-ceramic. We used a β-quartz solid solution glass-ceramic (Beall, 1989). The resistance to failure under uniaxial compression of samples which comply with the standard specification dimensions (106 mm length and 52 mm in diameter) is very high (greater than 450 MPa) and is beyond the load capacities of our press machine. Therefore, we selected a sample geometry, that deviates from our standard specification. The most informative fractographic results were obtained from a sample in the shape of a truncated cone 104 mm long (the part of a conical solid left after cutting off a top portion by a plane parallel to the base) having an elliptical cross section, such that the large and small diameters at the base end are 33 mm and 21 mm, respectively, and the two diameters at the top end of the truncated cone are respectively 33 mm and 10 mm. This shape was chosen in order to facilitate fracture at relatively low stresses. The abraded flexural strength of the β-quartz solid solution glass-ceramic is 69.3 MPa (Beall et al., 1967). The axial loads varied from 0 MPa up to 112 MPa (there was no confining pressure in this case).

Characteristics of EMR pulses along the stress–strain curve

We began our investigations in the study of individual EMR pulses excited by fractures of granite, chalk, and rhyolite. Our investigations showed that (Rabinovitch et al., 1996):

a. EMR pulses appear in two main forms: "lengthy" (total duration 30–110 μs and up to 400 μs) and "short" (0.5–6 μs).
b. An analysis of the EMR pulses emanating during uniaxial failure of rhyolite (Rabinovitch et al., 1996) showed that the deformation process can be divided into three zones according to the EMR features (Fig. 2):
   Zone I—of individual EMR pulses;
   Zone II—of EMR pulses with an uneven shape and/or groups of pulses;
   Zone III—of lengthy EMR pulses.
c. At the beginning of the deformation, individual pulses occurred, while at the upper part of the elastic zone the shape of the EMR events became more complex, indicating a superposition of individual pulses (sequences), with internal inter-pulse spacing of less than 3 μs. The interval between sequences was 40–80 μs.
d. Lengthy EMR pulses were registered immediately before and at the peak stress zone.
e. These results indicate a correlation between the EMR shapes and the failure stages. Thus, individual short pulses (Zone I) seem to be correlated with the stage of individual microcrack formation; multi-pulse sequences (Zone II) can be correlated with the crack coalescence stage; and the lengthy pulses (Zone III) can be correlated with the sample failure.

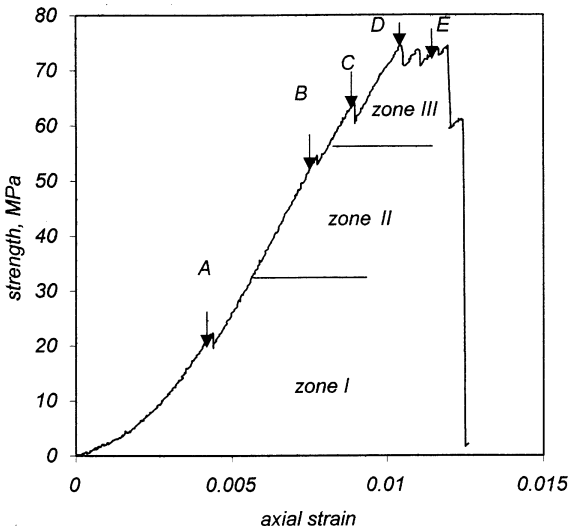

Fig. 2. Stress–strain curve of a rhyolite sample. Arrows on the graph show moment of EMR pulse excitation. Zone I is defined by individual pulses; Zone II is characterized by pulses with uneven shape and/or groups of pulses; Zone III shows particularly lengthy pulses (see elaboration of significance of arrows A–E in Rabinovitch et al., 1996).

Characterization of an individual EMR pulse and its correlation with crack sizes

Results show that an EMR pulse (voltage A vs. time t) can be characterized by the empirical general relationship shown in eq 1, below (Fig. 3a), where t is the time; t_0 is the time from the origin up to the pulse beginning; T is the time from the origin up to the EMR pulse envelope maximum. Thus, $T' = T - t_0$ is the time

$$A = \begin{cases} A_0 \sin(\omega(t - t_0))\,(1 - \exp(-(t - t_0)/\tau)) & t < T \\ A_0 \sin(\omega(t - t_0))\exp(-(t - T)/\tau)\,(1 - \exp(-(T - t_0)/\tau)) & t \geq T \end{cases} \quad (1)$$

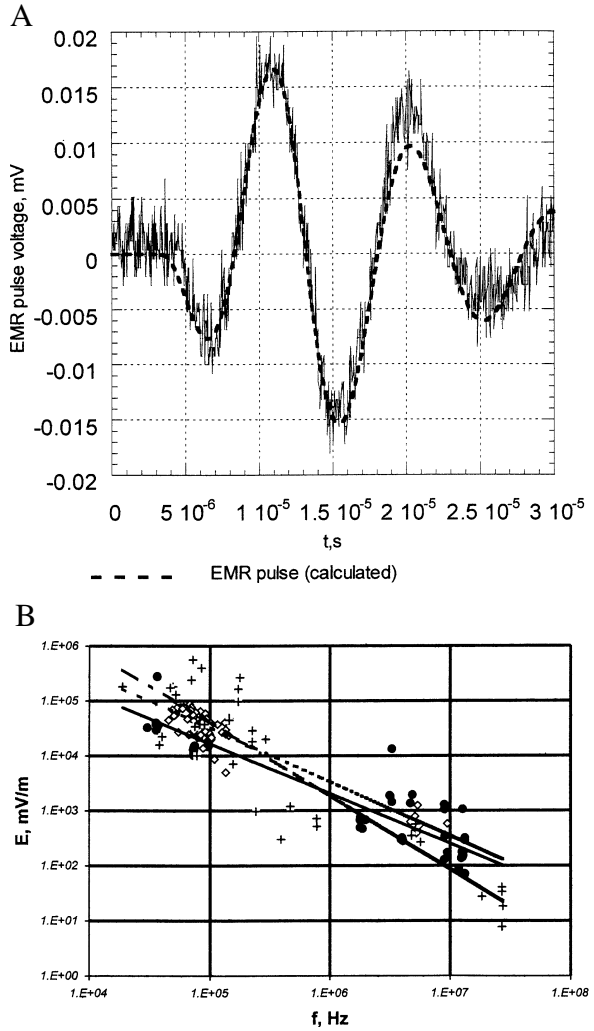

Fig. 3. A) An experimental EMR pulse and its numerical fit; B) Amplitude–frequency relation of EMR pulses associated with chalk, granite and glass-ceramic compression (• chalk; ◊ granite; + glass-ceramic; —— chalk trendline; --- granite trendline; –·– glass-ceramic trendline).

interval to reach pulse maximum; τ is the rise time and the fall time, which turn out to be the same; A_0 is the pulse amplitude and ω is the frequency. All these parameters except t (experimental variable) were calculated by a least-squares fit from the experimental results (Rabinovitch et al., 1998).

For the granite experiment, sixty EMR pulses were registered during all ranges of compressive loads up to the peak stress, and 55 were analyzed. Five were discarded, being too complex to analyze. An example of an EMR pulse with its least-squares fit is shown in Fig. 3a. As can be seen, both the accuracy of the measurement and that of the parametrization procedure are adequate.

This parametrization allowed us to derive and check very important results:

1. Relation between T′ and crack length. Denote the crack dimensions by l (length) × b (width) × u (aperture). We maintain that the pulse amplitude increases as long as the crack continues to grow, when new atomic bonds are severed and their contribution is added to the EMR. When the crack halts, pulse amplitude starts to decay. The time from pulse origin up to its maximum ($T' = T - t_0$) should be proportional to the number of severed atomic bonds and thus to the crack length l (assuming crack velocity to be almost constant).
2. The time interval T′ obeys a log-normal distribution. A possible explanation for this distribution can be as follows: T′ is proportional to crack length (from 1., above); if we assume that the fracture process develops incrementally and that each new increment is proportional to the existing crack length (as previously observed by Gillespie et al., 1992, and Cowie and Scholtz, 1992a,b), then a log-normal distribution should be expected (Aitchison and Brown, 1976).
3. The frequency of the EMR pulse relates to the crack width "b" by the following argument. We assume that the wavelength of atomic perturbation creating the EMR is limited by the crack width (since on both sides of the crack, atomic movements are restricted). Thus the frequency ω can be calculated by $\omega = \pi v/b$, where v is the wave velocity, and 2b is the wavelength (by the above restriction). As a check of this relation consider, e.g., the width of the smallest fracture in glass-ceramic, which was measured as about 3 mm; the corresponding frequency was 2.5 MHz. This implies a wave velocity of ~2500 m/s, which is in very good agreement with the Rayleigh velocity calculated by the measured elastic parameters.
4. No scaling of length with width. First, note that in usual crack experiments (e.g., Walmann et al., 1996), it is the aperture "u" (and not the width of the crack) which is compared to crack length l. Results show a fractal relation, $u \sim l^{\beta}$, where β ranges between 0.5 and 1. We tried to fractally correlate T′ and ω. $\omega \sim (T')^{-\nu}$, which would have implied a similar scaling between crack length and width; however, results show that the obtained ν is of the order of zero. This suggests that crack length is independent of its width or, alternatively, that the

width is constrained by some other mechanism, such as grain boundaries, intergranular spacings, etc. Similarly, Bahat (1988) noted that in geological fractures in chalks, in a given layer of constant width, there is a wide range of fracture lengths.

5. The amplitude of the envelope of the EMR pulse is, from eq 1 (Rabinovitch et al., 1998):

$$\bar{A} = A_0 (1 - \exp(-(T' / t)) \qquad (2)$$

and it was shown that the frequency f of the EMR pulses is inversely proportional to crack width. Since A_0 is proportional to crack area (which is a measure of severed bonds, each of which contributes to the EMR amplitude), it should be expected that

$$\bar{A} \propto \frac{1}{f} \qquad (3)$$

Voltage heights of EMR pulses also depend on antenna reaction (antenna efficiency), which changes with frequency. Compensating for this factor, $E = f(\bar{A})$ (E being the field amplitude reaching the antenna) by the appropriate antenna efficiency chart (EHFP-30 Near Field Probe set, Electro-Metrics Penril Corp.), we were able to compare various EMR signal heights of different frequencies.

Figure 3b shows the compensated amplitudes (E) of electromagnetic field signals induced by the fracture of chalk, granite, and glass-ceramic samples. Analysis of about 160 pulses shows that the amplitude–frequency ratio of each of the three materials can be fitted by a power law type relation. Note that the three curves appear close to each other. Thus, for chalk the fitted relation is:

$E \cong 6 \times 10^8 f^{-0.91 \pm 0.04}$

(squared regression coefficient $R^2 = 0.87$),

for granite:

$E \cong 3 \times 10^9 f^{-0.99 \pm 0.04}$ ($R^2 = 0.89$),

and for the glass-ceramic one:

$E \cong 2 \times 10^{11} f^{-1.32 \pm 0.11}$ ($R^2 = 0.82$).

If we collect all EMR data, a single combined relation can be obtained:

$$E \cong 5 \times 10^9 f^{-1.06 \pm 0.04} \ (R^2 = 0.84)$$

These results imply that the amplitude of the EMR field is really inversely proportional to the signal frequency and hence to crack width (Rabinovitch et al., 1998, 1999).

EMR and elastic parameters

As is presently known, an increase of elasticity, strength, and loading rate during uniaxial loading increases EMR amplitude (Gol'd et al., 1975; Nitsan, 1977; Khatiashvili, 1984). However, a study of electromagnetic radiation (EMR) emitted during triaxial compression has not been conducted. All our granite samples (Frid et al., 1999) passed through the "normal" three deformation stages (Jaeger and Cook, 1979) during compression up to the peak stress: (a) the nonlinear region of pore closure (the axial strain curve here is slightly bent down, (b) the elastic region (the stress–strain curves are quasilinear), and (c) the nonlinear region before the peak stress.

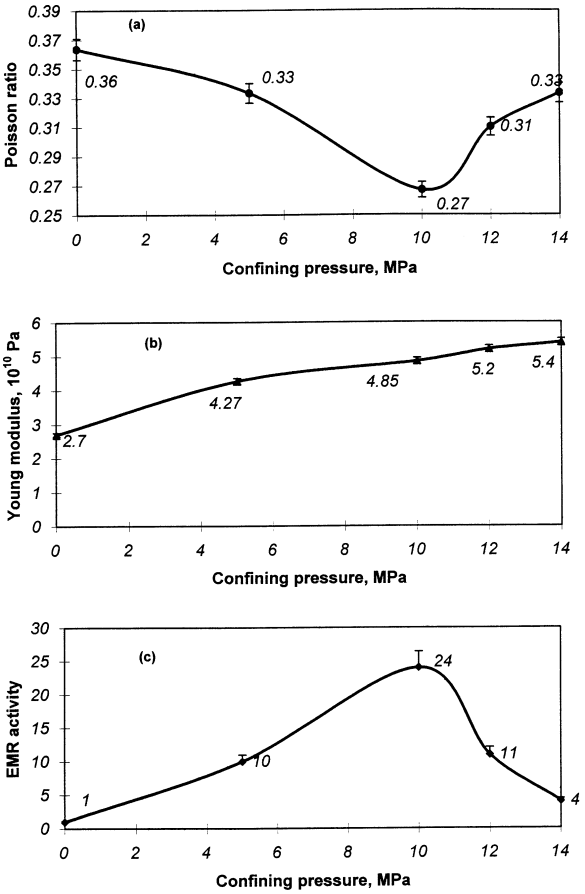

Fig. 4. Relationship of the following characteristics with confining pressure: (a) Poisson ratio; (b) Young's modulus; (c) EMR activity. Error bars in these figures are determined by the accuracy limits of our rock mechanics equipment, that is ±2% for Poisson ratio and Young's modulus and by the dead time of the storage oscilloscope–IBM-PC system (the period it takes for registration, digitizing, and memorizing an EMR sequence, during which the system is shut down). The error in EMR activity is of the order of +2%.

Our results show that the Poisson ratio (Fig. 4a) changes from 0.36 (for uniaxial test) via 0.27 for 10

MPa confining pressure to 0.33 for 14 MPa confining pressure. Young's modulus (Fig. 4b) increases monotonically from 27 GPa to 48.5 GPa with the confining pressure.

In our study, we denote EMR "activity" to be the number of individual EMR pulses emitted during tracing of the entire stress–strain curve. Its value is seen to change with loading type (Fig. 4c), increasing first with the confining pressure and then decreasing again. We checked 16 stress–strain characteristics to investigate possible correlations with EMR activity (listed in the Appendix). Our study shows that of all these stress–strain characteristics, the Poisson ratio is the only one that shows good correlation with EMR activity. Their squared regression coefficient was 0.93. An increase of the Poisson ratio (Fig. 4a) is accompanied by a decrease of EMR activity (Fig. 4c) and vice versa. Note that since all samples here are made of the same material (granite), the Poisson ratio varies only with loading conditions, and does not vary with material properties. Since Young's modulus increases monotonically with confining pressure (Fig. 4b), it is obvious that its correlation with EMR activity should be poor (the obtained squared regression coefficient was actually 0.18).

The correlation (or rather anti-correlation) of EMR activity with the Poisson ratio seems plausible. The Poisson ratio measures the compliance of the material in the transverse direction when stressed axially. The lower the Poisson ratio, the harder it is for the material to strain transversally, and hence the higher the probability of new fractures (especially parallel to the axis) and of the ensuing EMR. On the other hand, the higher the Poisson ratio the easier it is for the material to strain transversally, and accordingly, fewer fractures and lower EMR activity should be expected. The key elastic parameter for EMR characterization during triaxial compression is therefore the Poisson ratio and not Young's modulus. Although for uniaxial loading our results are in line with those of Gol'd et al. (1975) and Khatiashvilli (1984), which show an increase of EMR activity with Young's modulus, our triaxial results show the correct global parameter to choose. Khatiashvilli (1984) also indicates that the EMR activity correlates well with the lateral resistance to axial fracture, which is compensated by an increase in the number of new cracks.

Electromagnetic radiation of tensile vs. shear fractures

Yamada et al. (1989) measured EMR and acoustic emission (AE) during fracture of Indian granite. Acoustic emission larger than a preassigned threshold level was recorded. Some of these records showed an accompanying EMR. The initial phase of the AE signal was used to indirectly indicate the cracking mode. Thus a negative initial phase was associated with a shear mode, and a positive initial phase with a tensile one. Among 15 AE signals, accompanied by EMR, 14 were thus decided by Yamada et al. (1989) to be the result of tensile cracks, and only one of a shear crack. According to these authors, these results indicate that

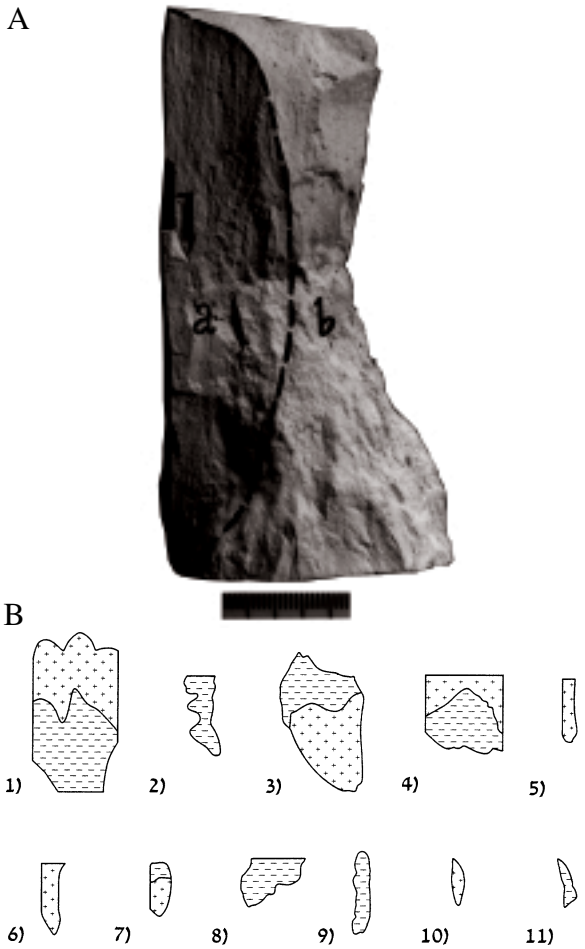

Fig. 5. (A) A photograph of a fractured surface on which the dashed line marks the boundary between the tensile part (a) showing planarity, gray tint, and strong striae, and the shear part (b) showing coarse topography, white color, and sugary texture. The tensile part is still covered by a piece of the shear part at the center of the sample (indicated by the "a" arrow). Scale in cm. (B) A graphic display of one of the samples that was fractured to 11 pieces, on which the tensile and shear areas were determined (+, tensile fracture; –, shear fracture).

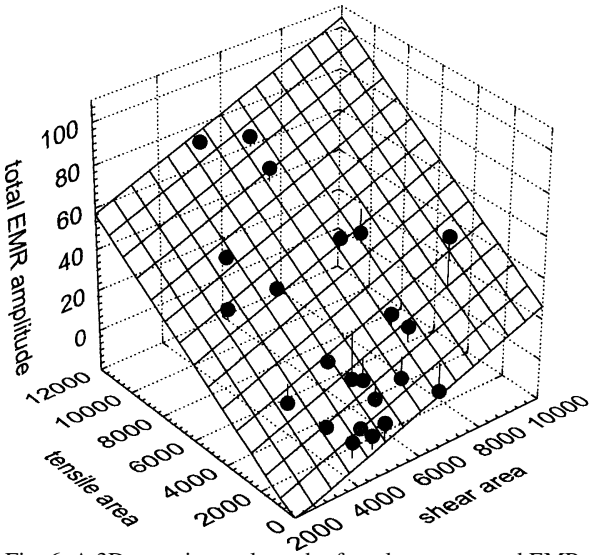

Fig. 6. A 3D experimental graph of total compensated EMR pulse amplitudes (V/m) versus total areas (mm^2) of tensile and shear crack areas of all investigated samples and their fit.

tensile cracking excites more intensive EMR than shear cracking. On the other hand, Petrenko (1993) suggested an EMR mechanism that is based on electrification of crack sides by friction. Since this effect is larger for a shear fracture than for a tensile fracture, this should imply the EMR amplitude to be much greater for the shear fracture. Our study considered the influence of tensile vs. shear fracture modes on EMR.

We selected chalk for our study because of its combined properties of low strength and micro-texture. These properties facilitated fracture at relatively low stresses, leading to a relatively small number of fragments at failure. As expected from our previous studies (Bahat, 1988), the fractured surfaces exhibited a useful fractography. It turned out that tensile fractures were planar and intensely marked by "striae" (plumes) (Bahat, 1979). These surfaces reflected a light grayish color. The shear fractures, on the other hand, have rough morphologies that were marked by white, coarse, "sugary" textures (Fig. 5a). The discrimination between these very distinct surfaces provided a fractographic criterion to distinguish between the two modes of fracture, and helped us to develop a method for the determination of tensile vs. shear fracture zones.

The total area of one wall of each fracture type was obtained by measuring all crack surfaces obtained for each sample and combining the sums for each type (Fig. 5b). Measurement errors varied from 3% to 8%. Twenty-three chalk samples were investigated under different loads. The first 11 samples were loaded uniaxially, while the 12 following ones were loaded triaxially. During the triaxial test, the lateral load was changed from 1 to 15 MPa, which caused a monotonic rise of sample strength from 37.7 MPa up to 80.1 MPa. Young's moduli for all tested samples changed from 6.2 up to 11.3 GPa, and the Poisson ratio from 0.07 up to 0.37.

As we noted above, EMR pulse amplitude increases as long as new atomic bonds are severed (Rabinovitch et al., 1998, 1999), hence this amplitude is related to the crack area. We compared the total amplitude (sum of compensated amplitudes) of the EMR pulses from each sample (measured above the sample's elastic limit) with the total respective areas (sums of crack areas of a given sample) of tensile and of shear cracks (Rabinovitch et al., 1999). Figure 6 shows 3D graphs of total compensated EMR pulse amplitudes vs. total areas of tensile and shear cracks of all investigated samples. The total EMR amplitude E was fitted by the linear equation: $E = -33.39 + 0.00655S_t + 0.00596S_s$ (with a squared regression coefficient $R^2 = 0.86$), where S_t and S_s are the total areas of tensile and of shear cracks of a given sample, respectively. The difference between the two coefficients multiplying S_t and S_s is of the order of ±5%, which is rather small and might be attributed to the error in area measurements (3–8% as noted above). This result shows that it is only the size of the entire area of the crack, irrespective of its mode, which governs the amplitude of the EMR.

CONCLUSION

As mentioned above, there is agreement in the literature that the "EMR technique" is a good candidate for future forecast of earthquakes. However, so far, all efforts to use EMR for earthquake prediction have met with very meager success due to the lack of a detailed quantitative understanding of the EMR mechanism (King, 1983; Rabinovitch et al., 1996). We assert that an essential step in the right direction should rely on obtaining a clear understanding of the physical phenomenon of EMR induced by fracture. The main merit of applying EMR to EQ prognosis is the sensitivity of this technique in the micro-scale (mm–cm): EMR is emitted from microcracks at their nucleation stage much before any rock displacement occurs. Therefore it is of great importance to master the correlation between EMR pulse signals and the size and shape parameters of the microcracks that produce these signals. An important part of this process is the understanding of the crack nucleation and evolution in the atomic scale. A reasonable background of understanding

EMR phenomena in the atomic and micro-scales would lead to experimental studies in macro-scales. An upscaling of laboratory experiments into a pilot-scale would be the next stage. Controlled/monitored fractures in quarries will constitute a logical step prior to a potential use of EMR in EQ prediction programs similar to the conventional seismic ones.

ACKNOWLEDGMENTS

We would like to thank the Israel Science Foundation founded by the Israel Academy of Sciences and Humanities, the Earth Sciences Administration of the Ministry of Energy and Infrastructure, and the "Ezvonot Committee" of the Israeli Government Estate Distributions for supporting our research. This work was also supported by the special funds from the Rector of the Ben-Gurion University of the Negev and the Dean of the Faculty of Natural Sciences. We thank George H. Beall of Corning Inc. (Corning, NY) for supplying glass-ceramic samples. We are grateful for technical help from Dr. V. Palchik, M. Barima, and D. Frid. We would like to thank the two anonymous reviewers for their comments, which helped considerably to improve the paper.

REFERENCES

Aitchison, J., Brown, J.A.C. 1976. The lognormal distribution. Cambridge University Press, Cambridge.

Bahat, D. 1979. Theoretical considerations on mechanical parameters of joint surface based on studies on ceramics. Geol. Mag. 116: 81–92.

Bahat, D. 1988. Fractographic determination of joint length distribution in chalk. Rock Mech. Rock Engin. 21: 79–94.

Bahat, D. 1991. Tectonofractography. Springer-Verlag, Heidelberg.

Beall, G.H., Karstetter, B.R., Rittler, H.L. 1967. Crystallization and chemical strengthening of stuffed β-quartz glass-ceramics. J. Am. Ceram. Soc. 50: 99–108.

Beall, G.H., 1989. Design of glass-ceramics. Rev. Solid State Sci. 3: 333–354.

Bella, F., Bjadji, P.F., Della Monica, J., Zilpimiani, D.O., Manguladze, P.V. 1992. Observations of natural electromagnertic radiation during earthquakes of central Italy. Izv. Earth Physics 28: 88–94.

Bogosh, R., Bourne, J., Shirav, M., Harnois, L. 1997. Petrochemistry of a Late Precambrian granitiferous granite, pegmatite and aplite, southern Israel. Miner. Mag. 61: 111–122.

Cowie, P.A., Scholtz, C.H. 1992a. Displacement–length scaling relationship for faults: data synthesis and discussion. J. Struct. Geol. 14: 1149–1156.

Cowie, P.A., Scholtz, C.H. 1992b. Growth of faults by the accumulation of seismic slip. J. Geophys. Res. 97: 11085–11095.

Drakopoulos, J., Stavrakakis, G.N., Latoussakis, J. 1993. Evaluation and interpretation of thirteen official VAN-telegrams for the period September 10, 1986 to April 28, 1988. Tectonophysics 224: 223–236.

Fifolt, D.A., Petrenko, V.F., Schulson, E.M. 1993, Preliminary study of electromagnetic radiation from cracks in ice. Philos. Mag. B 67: 289–299.

Frid, V. 1997a. Rock-burst hazard forecast by electromagnetic radiation excited by rock fracture. J. Rock Mech. Rock Engin. 30: 229–236.

Frid, V. 1997b. Electromagnetic radiation method for rock and gas outburst forecast. J. Appl. Geophys. 38: 97–104.

Frid, V., Rabinovitch, A., Bahat, D. 1999. Electromagnetic radiation associated with induced triaxial fracture in granite. Philos. Mag. Lett. 79: 79–86.

Fujinawa, Y., Takahashi, K. 1998. Electromagnetic radiations associated with major earthquakes. Phys. Earth. Planet. Inter. 105: 249–259.

Gershenzon N., Gokhberg, M., Morgunov, V. 1987. Sources of electromagnetic emissions preceding seismic events. Izv. Earth Phys. 23: 96–101.

Gershenzon, N., Gokhberg, M., Karakin, A. 1989. Modelling the connection between earthquake preparation processes and crustal electromagnetic emission. Phys. Earth Planet. Inter. 57: 129–138.

Gillespie, P., Walsh, J.J., Watterson, J. 1992. Limitations of displacement and dimension data for single faults and the consequences for data analysis and interpretation. J. Struct. Geol. 14: 1157–1172.

Gokhberg, M., Morgunov, V., Aronov, E. 1979. High frequency electromagnetic radiation during seismic activity. DAN SSSR 248: 1077–1081.

Gokhberg, M., Yoshino, T., Morgunov, V., Ogava, T. 1982. Results of recording of operative electromagnetic precursor in Japan. Izv. Earth Phys. 18: 144–146.

Gokhberg M., Gufel'd, I., Gershenzon, N. 1985. Electromagnetic effects due to crustal destruction. Izv. Earth. Physics 21, 52 – 63.

Gokhberg, M., Morgunov, V., Matveyev, V. 1986. On the observation of anomalous electromagnetic emission in the epicentral zone of earthquake. Izv. Earth Phys. 22: 676–678.

Gol'd, R.M., Markov, G.P., Mogila, P.G. 1975. Pulsed electromagnetic radiation of minerals and rock subjected to mechanical loading. Izv. Earth Phys. 7: 109–111.

Hayakawa, M., Tomizawa, I., Ohta, K. 1993. Direction finding of precursory radio emissions associated with earthquakes: a proposal. Phys. Earth Planet. Inter. 77: 127–135.

Jaeger, J.C., Cook, N.G.W. 1979. Fundamentals of rock mechanics. Chapman and Hall, London.

Jagasivamani, V., Iyer, K.J.L. 1988. Electromagnetic emission during the fracture of heat-treated spring steel. Mater. Lett. 6(11–12): 418–422.

Johnston, A.C. 1991. Light from seismic waves. Nature 354:

361.

Khatiashvili, N. 1984. The electromagnetic effect accompanying the fracturing of alkaline halide crystals and rocks. Izv. Earth. Physics 20: 656–661.

King, C.Y. 1983. Electromagnetic emissions before earthquakes. Nature 301: 377.

Misra, A. 1975. Electromagnetic effects at metallic fracture. Nature 254: 133–134.

Mogi, K. 1985. Earthquake prediction. Academic Press, New York.

Morgunov, V. 1985. Electromagnetic emission during seismic activity. Izv. Earth Phys. 21: 220–225.

Morgunov V., Matveyev, V. 1990. Electromagnetic emission in aftershocks of Spitak earthquake. Izv. Earth Phys. 26: 457–461.

Morgunov V., Matveyev, V. 1991. Electric and electromagnetic effects in the epicentral zone of Spitak aftershocks. Izv. Earth Phys. 27: 1002–1005.

Morgunov, V., Gerasimovich, E., Matveyev, V. 1988. Deformation of the earth surface and anomalous electromagnetic emission. Izv. Earth Phys. 24: 924–929.

Nesbitt, A.C., Austin, B. 1988. The emission and propagation of electromagnetic energy from stressed quartzite rock underground. Trans. Inst. Electr. Eng. 89: 53–56.

Nikiforova, N.N., Yadakhin, T.N. 1989. Studies of electromagnetic emission of tectonic origin in the Kirghiz SSR. Phys. Earth Planet. Inter. 57: 68–74.

Nitsan,V. 1977. Electromagnetic emission accompanying fracture of quartz-bearing rocks. Geotherm. Res. Lett. 4: 333–336.

O'Keefe, S.G., Thiel, D.V. 1995. A mechanism for the production of electromagnetic radiation during fracture of brittle materials. Phys. Earth Planet. Inter. 89: 127–135.

Ogawa, T., Oike, K., Miura, T. 1985. Electromagnetic radiation from rocks. J. Geophys. Res. 90: 6245–6249.

Parrot, M., Achache, J., Berthelier, J.J., Blanc, E. 1993. High frequency electromagnetic effects. Phys. Earth Planet. Inter. 77: 65–81.

Petrenko, V.F., 1993. On the nature of electrical polarization of materilas caused by cracks. Application to ice electromagnetic radiation. Philos. Mag. B 67: 301–315.

Rabinovitch, A., Bahat, D., Frid, V. 1995. Comparison of electromagnetic radiation and acoustic emission in granite fracturing. Int. J. Fract. 71: r33–r41.

Rabinovitch, A., Bahat, D., Frid, V. 1996. Emission of electromagnetic radiation by rock fracturing. Z. Geol. Wiss. 24: 361–368.

Rabinovitch, A., Frid, V., Bahat D. 1998. Parametrization of electromagnetic radiation pulses obtained by triaxial fracture in granite samples. Philos. Mag. Lett. 5: 289–293.

Rabinovitch, A., Frid, V., Bahat, D. 1999. A note on the amplitude–frequency relation of electromagnetic radiation pulses induced by material failure. Philos. Mag. Lett. 79: 195–200.

Sadovskii, M.A., Sobolev, G.A., Migunov, N.I. 1979. Changes of natural radiowave radiation during Karpatian eartquake. Dokl. Akad. Nauk SSSR 244: 316–319 (in Russian).

Urusovskaja, A.A. 1969. Electric effects associated with plastic deformation of ionic crystals. Sov. Phys-Usp. 11: 631–643.

Walmann T., Malthe-Sorenssen, A., Feder, J., Jossang, T., Meakin, P., Hardy, H.H. 1996. Scaling relations for the lengths and widths of fractures. Phys. Rev. Lett. 77: 5393–5396.

Warwick, J.W., Stoker, C., Meyer, T.R. 1982. Radio emission associated with rock failure: possible application to the great Chilean earthquake of May 22, 1960. J. Geophys. Res. 87: 2851–2859.

Yamada, I., Masuda, K., Mizutani, H. 1989. Electromagnetic and acoustic emission associated with rock fracture. Phys. Earth Planet. Inter 57: 157–168.

Yepez, E., Angulobrown, F., Peralta, J. 1995. Electric field pastterns as seismic precursors. Geophys. Res. Lett. 22: 3087–3090.

Yoshino, T., Tomizawa, I. 1989. Observation of low-frequency electromagnetic emissions as precursors to volcanic eruption at Mt. Mihara during November, 1986. Phys. Earth Planet. Inter. 57: 32–39.

Yoshino, T., Tomizawa, I., Sugimoto, T. 1993. Results of statistical analysis of low-frequency seismogenic EM emissions as precursors to earthquakes and volcanic eruptions. Phys. Earth Planet. Inter. 77: 21–31.

APPENDIX

The sixteen stress–strain characteristics that were investigated for possible correlation with EMR activity

1. Axial strain and its increment
2. Confining pressure
3. Deformation modulus (ratio of axial stress increment to rise of axial strain—the secant modulus) and its absolute value
4. Differential stress
5. Differential volumetric compression work (product of differential stress increment and volumetric strain changes) and its absolute value
6. Elastic strain work (product of average differential stress and elastic volumetric strain changes)
7. Elastic volumetric strain (part of volumetric strain that returns to its original value after applied stresses are removed)
8. Lateral deformation modulus (ratio of axial deformation increment to rise of lateral deformation—the secant lateral modulus) and its absolute value
9. Maximal stress
10. Poisson ratio (ratio of lateral elastic deformation to an axial elastic one, measured in the elastic zone of deformation)
11. Residual axial strain (remaining axial deformation after removal of external stress)
12. Residual strain work (strain work minus elastic work)
13. Residual volumetric strain (remaining value of the sum of the three principal strains after removal of external stress) and its absolute value
14. Strain work (product of average differential stress and volumetric strain changes) and its absolute value
15. Volumetric strain (sum of the three principal strains) and its absolute value
16. Young's modulus (ratio of axial stress increment to rise of elastic axial strain, measured in the elastic zone of deformation).